Brachytherapy 21 (2022) 229–237

BRACHYTHERAPY

Comparison of novel shielded nasopharynx applicator designs for intracavitary brachytherapy

Benjamin Insley[1,6,*], Ken Goldberg[2], Luc Beaulieu[3], Yunzhi Ma[4], Stephen McKinley[2], I-Chow Hsu[5], J. Adam Cunha[5]

[1] Department of Physics, Brown University, Providence, RI
[2] Industrial Engineering and Operations Research, University of California, Berkeley, CA
[3] Department of Physics, Université Laval, Quebec, Canada
[4] CHU de Quebec - Université Laval Research Center, Axe Oncologie, Quebec, Canada
[5] Department of Radiation Oncology, University of California, San Francisco, CA

ABSTRACT

PURPOSE: Nasopharyngeal brachytherapy is limited in part by the radiotolerance of nearby organs like the soft palate. This study explores several novel shielding designs for an intracavitary applicator to significantly reduce soft palate dose while adhering to the constraints of standard treatment procedure.

METHODS: The Monte Carlo code TOPAS is used to characterize each prototype under typical high-dose-rate treatment conditions. Mucosal surface dose maps are collected to evaluate the shields on their dose reduction to the central and soft palate planning points and uniformity in their shielding profile. Practicality with respect to patient comfort and pretreatment imaging is discussed. History-by-history standard deviations are calculated for each simulation.

RESULTS: A design with elliptical tubing containing bundles of tantalum wires provides the most significant attenuation with 39% and 27% dose reduction to the center and soft palate locations, respectively. Another design utilizing miniature lead spheres loaded into a constructed cavity shows 27% and 24% dose reduction to the same locations while providing more uniform shielding and several practical benefits. Both shields are designed to be completely removable for applicator insertion and pretreatment imaging. The mean and maximum standard error of relative dose measurements was 0.36 and 1.14 percentage points, respectively.

CONCLUSION: Each shielding design presented in this study provides a novel approach to safely and effectively shield healthy tissue during intracavitary nasopharyngeal brachytherapy. Analysis performed using Monte Carlo suggests that the design using metal spheres most practically shields the soft palate and should be advanced to the next stages of clinical optimization.

Keywords: Nasopharyngeal cancer; Intracavitary brachytherapy; Brachytherapy applicators; Monte Carlo dose modeling; Radiation shielding

Introduction

The standard radiotherapy treatment for nasopharyngeal cancer includes delivering 54−72 Gy of external beam radiation therapy (EBRT) for primary disease or 30−42 Gy for recurrent disease. Brachytherapy can also be used as monotherapy to treat localized recurrent disease but is often used as part of a definitive course of treatment following EBRT. The typical brachytherapy boost involves 5−7 Gy high-dose-rate (HDR) or 10−54 Gy low-dose-rate (LDR) [1]. The nasal canal provides a natural pathway for intracavitary brachytherapy. However, the close proximity of the soft palate to the source dwell locations makes it difficult to minimize the mucosal surface dose. Brachyther-

Received 16 July 2021; received in revised form 18 December 2021; accepted 20 December 2021

Disclosure: This work was partially funded from a scholarship by the American Association of Physicists in Medicine (AAPM) Summer Undergraduate Fellowship Program. One author reports grants from National Sciences and Engineering Council of Canada (NSERC) Grant Numbers: IRCPJ 491776-15 and RGPIN-2019-05038, during the conduct of the study.

☆ Research data are stored in an institutional repository and will be shared upon request to the corresponding author.

* Corresponding author. Department of Physics, Brown University, 69 Brown St., Providence, RI 02912. Tel.: +201-874-7112.

E-mail address: BAInsley@mdanderson.org (B. Insley).

[6] Present Address: Department of Radiation Physics, MD Anderson Cancer Center, 1400 Pressler St., Houston, TX 77030, USA.

1538-4721/$ - see front matter
https://doi.org/10.1016/j.brachy.2021.12.007

apy can be a very conformal treatment modality due to its high dose gradient, but current nasopharynx applicators (specifically the Rotterdam model [2,3]) fail to protect the soft palate during irradiation [4]. Few attempts have been made at altering the applicator design [4,5], and a current literature search reveals that no attempts have been made at introducing shielding.

In this study, we sought a shielded applicator that could significantly reduce the soft palate dose without significantly changing the overall dimensions and shape of the applicator, and the geometry of the source positions. The Monte Carlo radiation transport code Geant4 is particularly popular for its compatibility with CAD files for complex geometries and previous success in validation experiments [8–10], including validation for brachytherapy applications [11,12]. The user-friendly wrapper, TOPAS [6,7], streamlines the application of Geant4 to clinically relevant simulations. For this paper, TOPAS was used to simulate HDR brachytherapy of several different shielding designs within a Rotterdam-style nasopharynx applicator.

Methods and materials

Shielding designs

This section will begin with a discussion of the three shielding designs considered: (*1*) solid tungsten, (*2*) tantalum wires, and (*3*) small lead spheres. The body of each applicator prototype resembles the Rotterdam Nasopharynx Applicator (RNA) in shape and material. The curved, silicone rubber design allows for maneuvering around the patient's anatomy and artifact-free CT imaging once the applicator is in place. Just like the RNA, two source tubes run along the superior and posterior surface of the applicator. When inserted in the patient, these source tubes exit via the patient's nostrils. Unlike the RNA, each design we present here will have a novel shield inferior anterior to the source tubes blocking radiation towards the soft palate.

We started with a simple design that is easy to model, easy to manufacture, and provides dense shielding. Two cavities, separated by about 9 mm, have been hollowed out beneath the source tubes in the center of the applicator to make way for large metal blocks that stretch the length of the bridge (Fig. 1a). Space is left in between the shields to allow for existing holes that prevent suction between the applicator and the mucosa. Two versions of this design were tested: solid tungsten blocks (nickel-iron alloy, density 18.0 g/cc) and 3D-printed tungsten blocks (density 3.64 g/cc). Tungsten was chosen for the first version because of its significant photon attenuation characteristics and high density [13]. 3D-printed tungsten was evaluated for this shielding design to investigate the possibility of 3D-printing more complex shields.

This first design is most likely not clinically acceptable for two main reasons. First, the large solid blocks decrease the overall flexibility of the applicator. Second, the high electron density of the tungsten will lead to unacceptable CT imaging artifacts. However, solid block shielding provides a commonsense comparator to judge our more innovative shielding designs. The following shielding designs can be measured against the performance of this simple but impractical design.

To address the two main issues of the block design, we created two types of shielding that could be removed when necessary, for example, for applicator insertion and pretreatment imaging. The first implements removable bundles of tantalum wires (Fig. 1c). Instead of block cavities, silicone tubes are embedded within the applicator bridge and run parallel to the source tubes. These embedded tubes guide bundles of tantalum wires parallel to the paths of the sources to provide comprehensive shielding. The bridge of the applicator was rounded slightly to allow for the wire tubes to get closer to the source tracks for better coverage and to prevent the wires from getting stuck on sharp turns. In this design, four tubes will need to fit through the patient's nostrils.

Despite the shielding benefits of tungsten for the block design, tungsten is a very brittle metal, only becoming ductile at very high temperatures. Tantalum was selected to replace tungsten for this design due to its superior ductility at room temperature [14], similar atomic structure [15], and similar mass attenuation coefficient (only a 2% difference between tungsten and tantalum for the mean Iridium-192 photon energy of 380 keV according to NIST) [16].

Three versions of this wire design were modeled for analysis. The first two models fit wires in the same size tubes as the source tubes, using either 0.5 mm diameter wires or 1.0 mm diameter wires. The third version used larger, elliptical-shaped tubes with 0.5 mm wires to try and cover a larger portion of the radiation field. The differences between these three wire designs are shown in Fig. 1c.

The final design (Fig. 1d) we explored sought to spread out the shielding more homogeneously while also making the shielding structure more flexible. In a way, the block designs and wire designs were combined to provide dense shielding while also allowing a path for removing the shields as needed. A single large cavity was hollowed out in the base of the silicone bridge and two silicone tubes were implanted in the bottom of the bridge to allow access to the cavity. Just as in the wire design, these tubes would fit inside the nostrils along with the source tubes. However, for this design, miniature (0.5 mm diameter) metal spheres would be fed to the cavity through each tube and held in place using air pressure. Removing the shields is accomplished by reversing the air pressure. Furthermore, the primary advantage of this design is that this sea of small spheres provides shielding along most of the surface of the applicator and, depending on how tightly one packs the spheres, can better conform to the constricted geometry of the throat. Two versions of this design were analyzed: lead spheres and tungsten carbide (50% tungsten by mass) spheres.

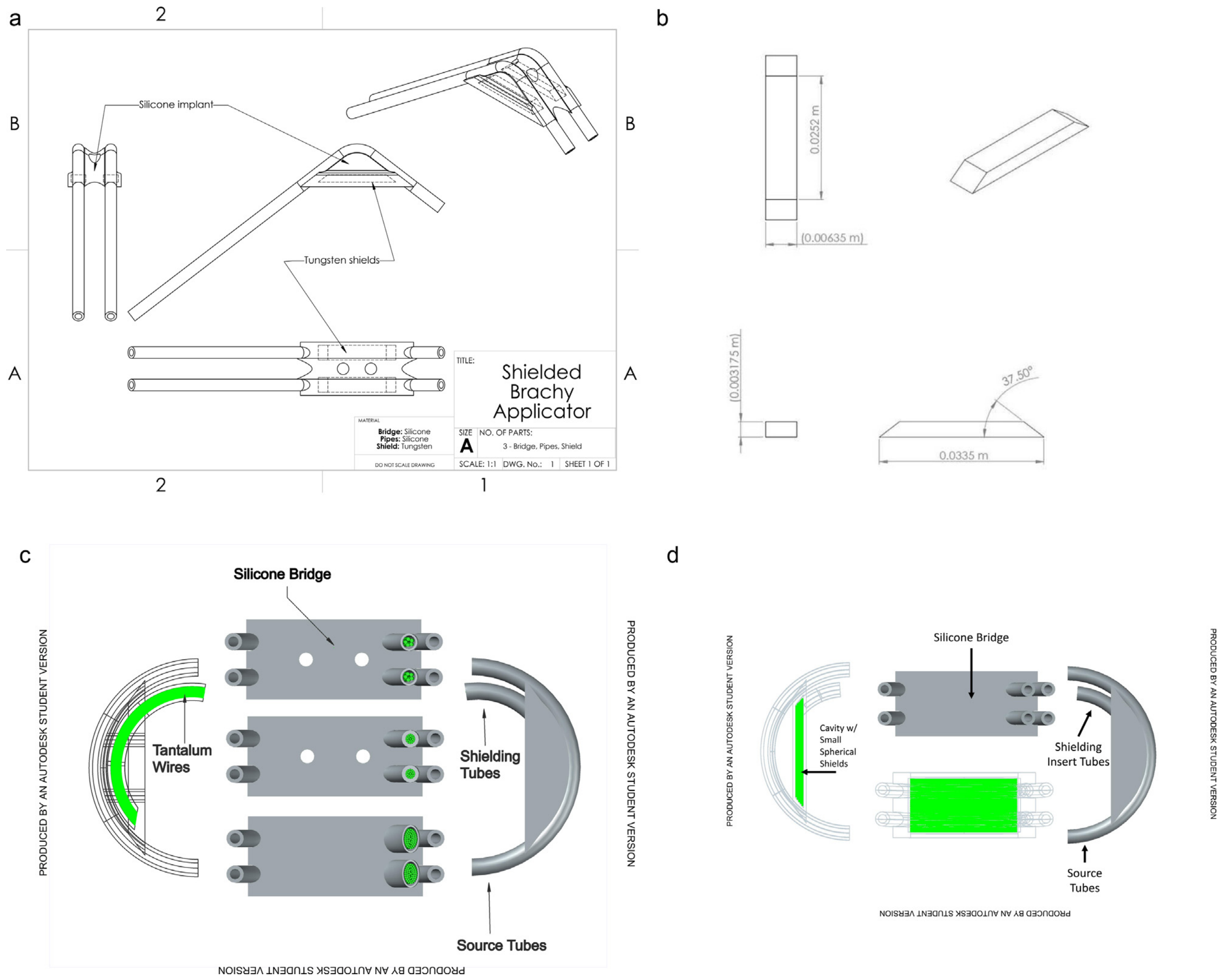

Fig. 1. (a) Block design schematic. A silicone rubber bridge encases two tungsten shields in the shape of trapezoidal prisms. Silicone tubes (outer diameter 5.0 mm and inner diameter 3.0 mm) run along the top of the applicator and guide the brachytherapy sources during treatment. When placed against the nasopharynx in the nasal canal, the shields face the soft palate while the sources run against the cancerous tissue. Refer to image b for scale. (b) Block Shield Dimensions. Both the solid tungsten shields and the 3D-printed tungsten/ABS plastic shields shared these dimensions. (c) Wire Design Schematic. The exterior geometry of the silicone bridge matches the block design in 1a except for the two extra silicone tubes added to house the wire shielding. The leftmost image shows how the wire tubes are embedded within the bridge beneath the source tracks. The three different versions of this design are shown in the middle with the 1.0 mm diameter wires on top, 0.5 mm diameter wires in the middle, and the wide 0.5 mm wires on the bottom. Each version's wire tubes follow the same trajectory, staying approximately 2 mm beneath the source tracks. The 0.5 mm and 1.0 mm wire tubes have the same inner and outer radius as the source tubes (3.0 and 5.0 mm, respectively). The elliptical-shaped tubes of the wide design have an inner minor axis of 3.75 mm and inner major axis of 6.0 mm. The distance between the two shielding tubes was shortened from 5 mm in the first two versions to 2 mm in the wide design. (d) Sphere Design Schematic. The exterior geometry again matches that of the block design in 1a except the block cavities have been extended to cover the bottom of the applicator. The leftmost image shows how the inner tubes feed into the embedded cavity. The green shielding block appears as a single volume, but is in fact composed of hundreds of 0.5 mm diameter spheres stacked within the bridge. The inner cavity is 2.8 mm tall and 19.0 mm wide. (For interpretation of the references to colour in this figure legend, the reader is referred to the web version of this article.)

See Supplementary Material Table I for a summary of the characteristics of the various materials used in each prototype.

Simulation procedure

The aim of simulation was to understand the dose reduction to normal tissue for each shielding prototype compared to treatment with no shielding. Each design was modeled in AutoCAD and imported into TOPAS (version 3.4, wrapped on Geant4 version 10.05.p02) as .stl files. The 3D image rendering software MeshLab was used to remove overlapping vectors. High resolution geometry can cause particle trajectory errors in Monte Carlo simulations, but with MeshLab we were able to maintain errors to less than 0.00025% of primary histories.

The simulation geometry is shown in Fig. 2. An Iridium-192 source was modeled after the Elekta micro Selectron HDR v2 specifications [17]. One source was placed in the top center of each of the two source tubes. A 3 cm

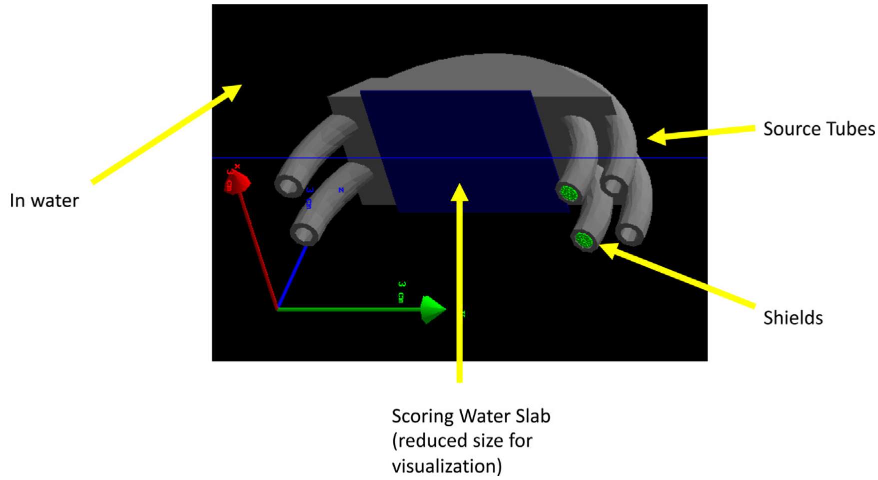

Fig. 2. Simulation geometry. An example of the experimental setup in TOPAS for the 0.5 mm wire design. The large blue slab on the bottom of the applicator represents the placement of the scoring volume (though its size is reduced for visualization). The Iridium-192 sources are placed in the top center of the outer tubes (marked source tubes). In this particular design, the tubes on the right side (the side of the tube labels) would exit out of the nose. The surrounding volume is composed of water. (For interpretation of the references to colour in this figure legend, the reader is referred to the web version of this article.)

x 6 cm scoring plane was placed flush to the bottom of the applicator where the soft palate would be in a typical treatment [1]. The thickness of the plane was set to 0.278 mm to match the thickness of a slice of Gafchromic EBT3 film [18], which is a typical dosimetry tool used for brachytherapy applicator experiments. In addition, this thickness provided high enough signal for adequately-low variance. Each experiment was set in a $40 \times 40 \times 40$ cm^3 cubical volume of water. A total of one billion (10^9) histories (500 million from each source) were simulated for each applicator design. Mean dose per particle was scored in 1.0×1.0 mm^2 voxels using a track length estimator [12] while standard deviations of each voxel were calculated using history-by-history uncertainty analysis. The default physics settings in TOPAS were used, including the Geant4 electromagnetic physics module, G4EMStandardPhysics_option4 [6,7]. With such large voxels compared to the max electron range for an Iridium-192 source, electron tracking was deprecated and their energy deposited locally.

Evaluation metrics

Each shield design required slight variations in applicator geometry which introduced uncertainties when combining the CAD applicator/shield volumes with the scoring plane/source TOPAS volumes. Though the placement errors were kept to within 3 mm both translationally and longitudinally, we corrected for these misalignments by running individual control simulations for every design that required different applicator geometries. The control simulations were created simply by switching the shield material to silicone while keeping all other parameters the same. With these control simulations, we present all of our metrics normalized by the respective control results. In this way we can more accurately compare shield efficacies without introducing significant inverse square law effects.

For each design, we first give two-dimensional maps of the dose and dose transmission. The dose maps are normalized by the maximum dose to 1×1 mm^2 in the corresponding control map. These maps help visualize the spatial distribution of the dose due to distance and shielding. Higher percentages indicate higher dose and vice versa. The dose transmission maps are the shielded map divided elementwise by the control map, thus giving one-to-one voxel normalization. This normalization isolates the effect of the shield presence for direct shield comparisons. Higher percentages indicate less shielding and vice versa.

To summarize the performance of each shield we provide three metrics. The first is the dose to the center of the dose map normalized by the corresponding voxel in the respective control dose map. The second is the dose to the soft palate planning point defined in Levendag *et al.* [2] where the Rotterdam Nasopharynx Applicator was introduced. This point is bilateral on the central horizontal axis of the scoring plane 1 cm from the central vertical axis. The soft palate dose will be presented as the average of these doses normalized by the control map points. The final metric is the field flatness given by $100 \times \frac{D_{Max}-D_{Min}}{D_{Max}+D_{Min}}$ where $D_{Max/Min}$ are the maximum and minimum doses within the central 2 cm of the dose map normalized by the control map. This gives a measure of how uniform the dose transmission is within the soft palate planning points, where lower percentages indicate more uniform dose reduction. Though dose reduction is the highest-priority metric for this study, flatness gives an indication of how sensitive the design is to shielding misalignment. Greater heterogeneity, that is,

Table 1
Shield performance under planning metrics

	Central dose (%)	Soft palate dose (%)	Flatness (%)
3D-printed tungsten blocks	100.78	94.62	4.32
Solid tungsten blocks	94.56	54.25	43.83
0.5-mm wires	98.95	99.03	13.87
1.0-mm wires	97.61	99.42	14.23
Wide wires	60.64	73.11	9.35
Lead spheres	73.49	75.99	2.30
TC sphere	80.90	81.68	2.31

TC = tungsten carbide.

higher values of flatness, will be more sensitive to inaccurate placement of the shields with respect to the sources and relevant anatomy.

Finally, to visualize how each design compares to one another, we provide dose volume histograms and central axis line profiles of the dose transmission maps. Because these plots are calculated from the dose transmission maps, the performance of each shield is normalized to the respective control allowing accurate comparison of the shielding performance.

Results

Figure 3 presents the dose maps and dose transmission maps of the lead sphere design (3b) and the simpler tungsten block design for comparison (3a). All dose maps and dose transmission maps are recorded in Supplemental Material Fig. 1. The color range for each map is kept constant at [0,100] percent for every plot for easy visual comparisons. The color bar in each figure therefore does not represent the range of the map.

With 10^9 primary histories, uncertainty in the dose maps was kept to a mean of 0.12 percentage points and a maximum of 0.40 percentage points. Uncertainty in the dose transmission maps was 0.36 percentage points on average and 1.14 percentage points at maximum. These uncertainties are presented in units of ‘percentage points’ to indicate that they are absolute uncertainties, that is, if a voxel received a relative dose of 70%, the margin of error around this dose is presented as 70 ± 0.12.

Figure 4 contains the dose transmission DVHs and dose transmission line profiles of all the prototypes. Line color and style are kept consistent between the two graphs. In each graph, when the dose is given as “Percent of Control Dose (1 to 1)”, this indicates that the dose was normalized by the corresponding control voxel.

Finally, Table 1 summarizes the planning metrics recorded from the dose transmission maps. Each percentage, except for the flatness score, represents the dose in the shielded trial normalized by the dose in the respective control. Thus, lower percentages indicate better shielding. Flatness is given in the last column, and it represents the deviation from homogeneous shielding. Lower percentages here indicate a more homogeneous dose reduction.

Discussion

When comparing these shields, the main questions we ask of each design are:

1. How well does it shield the soft palate from radiation?
2. How uniform is the shielding?
3. Can this design reasonably meet the standards of patient comfort that the Rotterdam Nasopharynx Applicator adheres to?
4. Can we perform all the necessary pretreatment imaging/quality assurance with this shielding design?

The last two questions are only speculative at this point given the theoretical nature of these simulations and will be important considerations in the next phase of research.

We begin with the block implants described first in the methods section. The 3D-printed tungsten blocks perform the worst in terms of shielding, providing just a 5% reduction in dose to the soft palate. This can be visualized in the corresponding transmission dose map (Supplementary Material Fig. 1c) where the primary shielding region is hardly visible. The only metric where this shielding performs well is field flatness, but this is simply due to lack of significant photon attenuation in the shields.

The central dose seen for the 3D-printed tungsten blocks demonstrates an interesting phenomenon. The dose measured when using the 3D-printed shields was greater by 0.8 percentage points (2.5 standard deviations) than that measured without any shielding. To investigate this further, we reran simulations of this design and the control without scoring scattered photons (Supplemental Material Fig. 2). The scoring plane only counted dose depositions from primary photon events. This resulted in a full standard deviation decrease (0.3 percentage points) in the difference between the center voxels of the shielded and unshielded dose maps.

We can consider these results from the perspective of the dominant photon interaction at the average Iridium-192 gamma energy (380 keV) for low Z materials like plastic: Compton scattering. The amount of Compton scattering should be increased in the 3D-printed shields compared to the control due to the higher electron density. How-

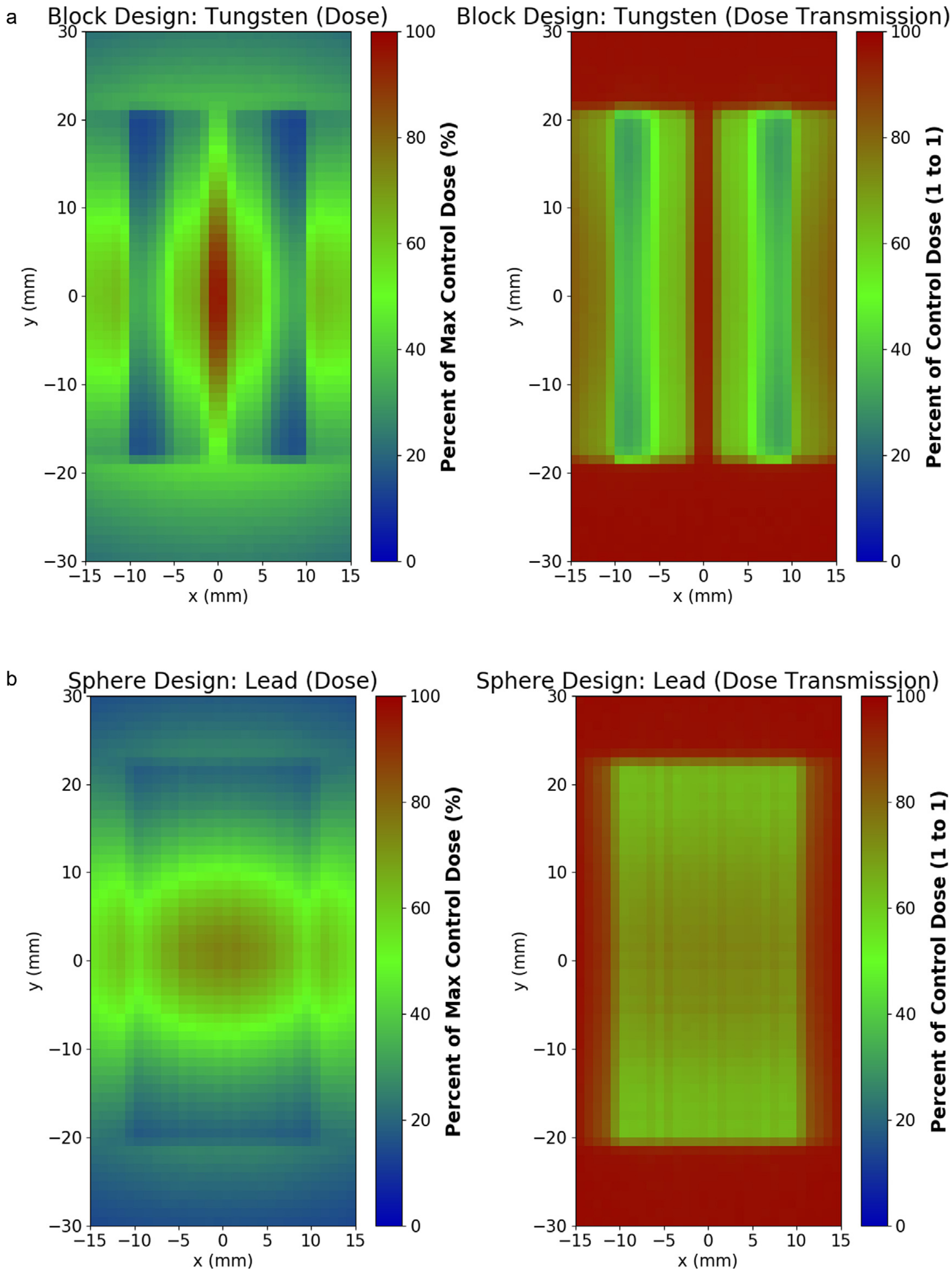

Fig. 3. Dose maps and transmission dose maps for select designs. The dose maps are created by normalizing the measured dose by the maximum dose of the corresponding control dose map, that is, $Dose(x, y) = \frac{Dose_{shielded}(x,y)}{max(Dose_{control}(x,y))}$. The transmission dose maps are normalized voxel by voxel with the respective control, that is, $Dose\ Transmission(x, y) = \frac{Dose_{shielded}(x,y)}{Dose_{control}(x,y)}$. Red indicates higher dose and blue indicates lower dose in the dose maps while red indicates less shielding and blue indicates higher shielding in the transmission dose maps. Dose maps and transmission dose maps for all other designs are included in Supplementary Figure 1.
(a) Solid Tungsten Block Shields.
(b) Lead Spheres. (For interpretation of the references to colour in this figure legend, the reader is referred to the web version of this article.)

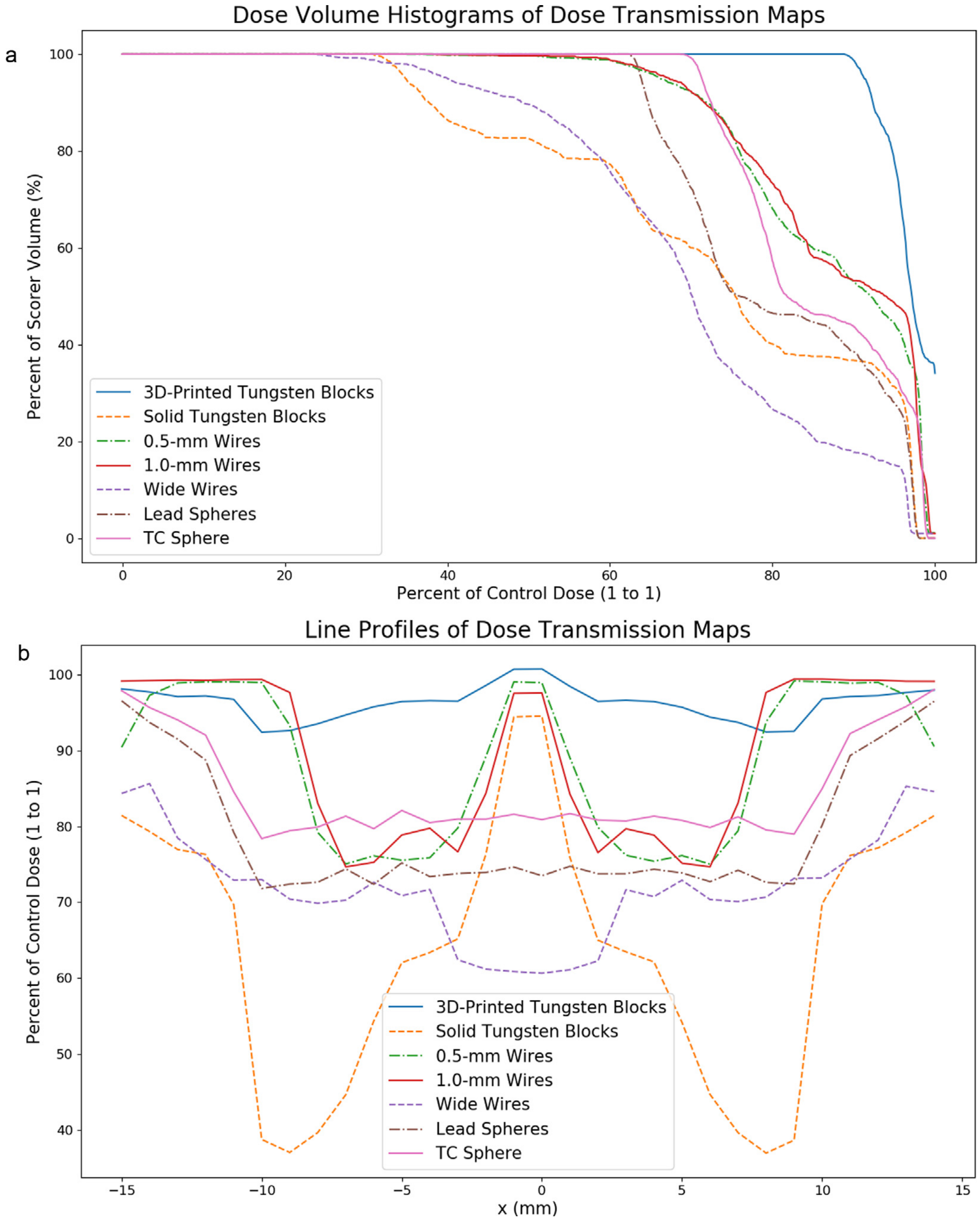

Fig. 4. (a) Dose volume histogram of transmission dose maps. (b) Central axis line profiles of transmission dose maps.

ever, the mass density of the 3D-printed shields is greatly reduced from that of the solid tungsten blocks (3.64 g/cc compared to 18.0 g/cc) due to the presence of ABS plastic in the shield composition. It appears that the photons are not being absorbed like they are in all the other shields, but rather being preferentially scattered. The increased dose is then due to the accumulation of scatter from the bilateral source positions in the gap between the shields. This highlights the danger of a shield geometry that incorporates a central gap. If 3D-printing is to be used for shield designs, the geometry has to carefully consider scattering due to its low density.

It must be noted that, even when accounting for scattering, the 3D-printed tungsten blocks still see a slightly greater dose in the center of the scoring plane compared to the control. Taking this into consideration, we will quote the uncertainty as 2 standard deviations (i.e., a 95% confidence interval), or 2.28 percentage points for the dose transmission maps. Shielding differences below this threshold will not be considered significant.

The solid tungsten blocks, on the other hand, outperform all other designs in lowering the soft palate dose. Table 1 reports that the solid tungsten blocks reduce soft palate dose by 46% compared to the control. However, this shielding is highly heterogeneous given the distance of the shields from the sources and the gap between the blocks. The central dose is 95% of the control's center - a much smaller reduction compared to that directly beneath the shields. This heterogeneous performance is summarized in the flatness calculation where this design provides the worst performance at 43.83%. Though solid tungsten blocks provide great attenuation, this design shows us that the shielding must cover more of the radiation field in order to be useful.

The 0.5 mm and 1.0 mm wire designs attempt to address this without adding much more material. Because the tantalum wires add flexibility to this design, we were able to move the shielding much closer to the source tracks. This allows less shielding to cover more of the radiation field due to the increased solid angle. However, the dose maps of Supplementary Material Fig. 1d and 1e show that the lateral shielding is still as weak as the tungsten bocks. In addition, 0.5 mm and 1.0 mm wires clearly do not cover enough area when fit inside tubes the same size as the sources. Their thinner profiles give dose transmissions over 95% in both the soft palate and central dose points. Directly beneath the shields, however, the line profile shows dose reductions near 25%. There is no significant difference between the 0.5 mm and 1.0 mm wires.

This leads us to the wide wire design, which seeks to address the inadequate lateral shielding of the 0.5 mm and 1.0 mm wire design. The central dose hotspot present in all the previous dose maps is eradicated in this design, as seen in the dose map of Supplementary Material Fig. 1f. The soft palate dose is higher than with the solid tungsten blocks at 73%, but the central dose is the lowest of all the designs at 60%. In addition, the field is much flatter than the blocks at 9.35%.

The third design incorporates small metallic spheres. The tungsten carbide (TC) spheres perform slightly worse than the lead spheres under all metrics, so we address only the lead spheres here. However, it should be noted that there has been research into versions of tungsten carbide with larger percentages of tungsten by mass than that modeled here. In particular, AbuAlRoos *et al.* found the shielding ability of tungsten carbide (at 98.65% tungsten) exceeds that of lead for energies less than 400 keV. The present study's results should be interpreted as a consideration of the miniature sphere geometry for a high-Z (lead) shield versus a low-Z shield (low-purity tungsten carbide). In later stages of development, dosimetric and non-dosimetric differences, such as environmental toxicity, cost, and machinability, between high-Z shields like lead and high purity tungsten will be considered [19]. The current shielding selections reflect a broad search of the present parameter space.

Looking at the dose and dose transmission maps of Fig. 3b, it is clear that this design provides the most homogeneous shielding. This is reflected in its 2.30% flatness measurement that far surpasses the other designs. The DVH and line profile shown in Fig. 4 demonstrate that this implant sits in the middle ground between the 0.5 mm/1.0 mm wire designs and the wide wire design. Its dose reduction in both the center and soft palate points is much better than the 0.5 mm/1.0 mm wires, but slightly worse than the wide wires. Overall, this shielding design has the best tradeoff between dose uniformity and dose reduction.

In terms of the last two questions presented at the beginning of this section, the sphere design has some notable advantages over the rest. Both patient comfort and pretreatment imaging require that the shields be removable. If the shields are removable, the applicator can be inserted and images can be taken prior to the introduction of metal. This requirement rules out the embedded block design, as previously discussed. The wire designs, however, are still viable. Though two extra tubes would need to fit inside the patient's nostrils, bundles of these tantalum wires can be inserted and removed as necessary. However, the most effective design, that is, the wide wires, introduces a lot more material into the patient's nasal canal. Though this prototype has the most impressive shielding performance, it might push the limits of patient comfort. In addition, we expect some difficulties fitting wires through silicone tubes reproducibly. The procedure may become tricky depending on how much shielding is used and how much friction is encountered.

The sphere design, however, is not limited by the size of the entrance tube. Because the spheres are being loaded into a cavity, they can be fed through the tube in a singulated method if needed. In addition, since the dimensions of the spheres are so much smaller than the wires, they can better conform to any necessary shape. Depending on the amount of shielding loaded into the cavity, we can allow some flexibility in the applicator, helping it to fit within the patient cavity. In future implementation of such a design, special consideration may be required to ensure spheres are loaded in a consistent, unimposing manner.

Conclusion

After simulation and evaluation of seven shielding prototypes in TOPAS, the prototype using small lead spheres shows the most promise. This novel applicator design has the potential to significantly reduce normal tissue dose and provide uniform shielding over the central portion of the field. Further work is needed to optimize the applicator geometry for the clinic, study patient comfort and pretreatment imaging, and develop rigorous dosimetry for accurate treatment planning, but this study has revealed that this novel design has potential for superior organ sparing and improved treatment outcomes.

Acknowledgments

Many thanks to Dr. Oludurotimi Adetunji for his guidance during my undergraduate senior thesis work. His mentorship certainly brought this work and my own education to greater heights. Thank you to the American Association of Physicists in Medicine for providing me with the opportunity to connect with Dr. Cunha at UCSF. Thank you to Brown University's High Performance Computing center for providing computational resources.

Supplementary materials

Supplementary material associated with this article can be found, in the online version, at doi:10.1016/j.brachy.2021.12.007.

References

[1] Lee N, Hoffman R, Phillips TL, *et al.* Managing nasopharyngeal carcinoma with intracavitary brachytherapy: one institution's 45-year experience. *Brachytherapy* 2002;1:74–82. doi:10.1016/s1538-4721(02)00013-2.

[2] Levendag PC, Peters R, Meeuwis CA, *et al.* A new applicator design for endocavitary brachytherapy of cancer in the nasopharynx. *Radiother Oncol* 1997;45:95–98 PMID: 9364638. doi:10.1016/s0167-8140(97)00105-9.

[3] Levendag PC, Vikram B, Flores AD, *et al.* High dose rate brachytherapy for cancer of the head and neck. In: Nag S, editor. High dose rate brachytherapy: a textbook. Armonk, NY: Futura Publishing Co.; 1994. p. 237–73.

[4] Bacorro WR, Agas RAF, Cabrera SMR, *et al.* A novel applicator design for intracavitary brachytherapy of the nasopharynx: simulated reconstruction, image-guided adaptive brachytherapy planning, and dosimetry. *Brachytherapy* 2018;17:709–717 Epub 2018 May 11. PMID: 29759328. doi:10.1016/j.brachy.2018.03.004.

[5] Chen Z, Li R, Wang P. Analysis of 80 cases of nasopharyngeal carcinoma treated by intracavitary brachytherapy using a new-type applicator. *Chin J Clin Oncol* 2007;4:52–55. doi:10.1007/s11805-007-0052-5.

[6] Perl J, Shin J, Schumann J, *et al.* TOPAS: an innovative proton Monte Carlo platform for research and clinical applications. *Med Phys* 2012;39:6818. doi:10.1118/1.4758060.

[7] Faddegon B, Ramos-Mendez J, Schuemann J, McNamara A, Shin J, Perl J, Paganetti H, The TOPAS Tool for Particle Simulation, a Monte Carlo Simulation Tool for Physics, Biology and Clinical Research, Physica Medica, doi:10.1016/j.ejmp.2020.03.019.

[8] Peterson S, Polf J, Ciangaru G, *et al.* Variations in proton scanned beam dose delivery due to uncertainties in magnetic beam steering. *Med Phys* 2009;36:3693–3702. doi:10.1118/1.3175796.

[9] Paganetti H, Jiang H, Lee SY, *et al.* Accurate Monte Carlo simulations for nozzle design, commissioning and quality assurance for a proton radiation therapy facility. *Med Phys* 2004;31:2107–2118. doi:10.1118/1.1762792.

[10] Archambault L, Arsenault J, Gingras L, *et al.* Plastic scintillation dosimetry: optimal selection of scintillating fibers and scintillators. *Med Phys* 2005;32:2271–2278. doi:10.1118/1.1943807.

[11] Poon E, Reniers B, Devic S, *et al.* Dosimetric characterization of a novel intracavitary mold applicator for 192Ir high dose rate endorectal brachytherapy treatment. *Med Phys* 2006;33:4515–4526. doi:10.1118/1.2364054.

[12] Francisco Berumen, Yunzhi Ma, Jose Ramos-Mendez, Joseph Perl, Luc Beaulieu. "Validation of the TOPAS Monte Carlo toolkit for HDR brachytherapy simulations." Brachytherapy (in press). doi:10.1016/j.brachy.2020.12.007.

[13] McAlister D. Gamma ray attenuation properties of common shielding materials. PG Research Foundation, 2018. Available at: https://www.eichrom.com/wp-content/uploads/2018/01/gamma-ray-attenuation-white-paper-by-d.m.-rev-4.pdf, last accessed on June 30, 2021.

[14] Pan Z. Comparative study of the effect of impurities on the ductility of tantalum and tungsten based on atomistic and first principles calculations. The University of North Carolina at Charlotte, Charlotte, NC, 2012.

[15] National Center for Biotechnology Information PubChem Compound Summary for CID 23956. *Tantalum* 2021. Available at: https://pubchem.ncbi.nlm.nih.gov/compound/Tantalum Accessed February 16, 2021.

[16] Atwell W, Rojdev K, Aghara S, Sriprisan S. Mitigating the Effects of the Space Radiation Environment: a novel approach of using graded-Z materials. In: AIAA SPACE 2013 conference and exposition; 2013.

[17] ESTRO. Ir-192 Hdr sources; 2019, last accessed on June 30, 2021.

[18] Gafchromic. 2019. "Gafchromic dosimetry media, type Ebt-3." Available at: http://www.gafchromic.com/documents/EBT3_Specifications.pdf, last accessed on June 30, 2021.

[19] AbuAlRoos N.J., Azman M.N., Amin N.A.B., Zainon R., Tungsten-based material as promising new lead-free gamma radiation shielding material in nuclear medicine, Physical Medica, doi:10.1016/j.ejmp.2020.08.017.